TISSUE ENGINEERING: Part A
Volume 26, Numbers 3 and 4, 2020

DOI: 10.1089/ten.tea.2019.0126

termis
Tissue Engineering
& Regenerative Medicine
International Society

ORIGINAL ARTICLE

Long-Term Evaluation of Functional Outcomes Following Rat Volumetric Muscle Loss Injury and Repair

Ellen L. Mintz, MS,[1] Juliana A. Passipieri, PhD,[2] Isabelle R. Franklin, BS,[3] Victoria M. Toscano, BS,[2] Emma C. Afferton, BS,[2] Poonam R. Sharma, PhD,[2] and George J. Christ, PhD[2,4]

Volumetric muscle loss (VML) injuries, by definition, exceed the endogenous repair capacity of skeletal muscle resulting in permanent structural and functional deficits. VML injuries present a significant burden for both civilian and military medicine. Despite progress, there is still considerable room for therapeutic improvement. In this regard, tissue-engineered constructs show promise for VML repair, as they provide an opportunity to introduce both scaffolding and cellular components. We have pioneered the development of a tissue-engineered muscle repair (TEMR) technology created by seeding muscle progenitor cells onto a porcine-derived bladder acellular matrix followed by cyclic stretch preconditioning before implantation. Our work to date has demonstrated significant functional repair (60–90% functional recovery) in progressively larger rodent models of VML injury following TEMR implantation. Notwithstanding this success, TEMR implantation in cylindrically shaped VML injuries in the tibialis anterior (TA) muscle was associated with more variable functional outcomes than has been observed in sheet-like muscles such as the latissimus dorsi. In fact, previous observations documented a dichotomy of responses following TEMR implantation in a rodent TA VML injury model; with an $\approx$61% functional improvement observed in fewer than half (46%) of TEMR-implanted animals at 12 weeks postinjury. This current study builds directly from those observations as we modified the geometry of both the VML injury and the TEMR construct to determine if improved matching of the implanted TEMR construct to the surgically created VML injury resulted in increased functional recovery posttreatment. Following these modifications, we observed a comparable degree of functional improvement in a larger proportion of animals ($\approx$67%) that was durable up to 24 weeks post-TEMR implantation. Moreover, in $\approx$25% of all TEMR-implanted animals, functional recovery was virtually complete (TEMR max responders), and furthermore, the functional recovery in all 67% of responding animals was accompanied by the presence of native-like muscle properties within the repaired TA muscle, including fiber cross-sectional area, fiber type, vascularization, and innervation. This study emphasizes the importance of tuning the application of tissue engineering technology platforms to the specific requirements of diverse VML injuries to improve functional outcomes.

Keywords: skeletal muscle, tissue engineering, volumetric muscle loss, wound healing

Impact Statement

This report confirms and extends previous observations with our implantable tissue-engineered technology platform for repair of volumetric muscle loss (VML) injuries. Based on our prior work, we addressed factors hypothesized to be responsible for significant outcome variability following treatment of VML injuries in a rat tibialis anterior model. Through customization of the muscle repair technology to a specific VML injury, we were able to significantly increase the frequency at which functional recovery occurred, and furthermore, demonstrate durability out to 6 months. In addition, the enhanced biomimetic qualities of repaired muscle tissue were associated with the most robust functional outcomes.

Departments of [1]Pathology, [2]Biomedical Engineering, [3]Biology, and [4]Orthopaedics, University of Virginia, Charlottesville, Virginia.

Introduction

Skeletal muscle has an extensive capacity for repair and regeneration following a variety of injuries.[1–4] Skeletal muscle repair is accomplished through proliferation and differentiation of satellite cells into myoblasts and multinucleated myotubes.[5–8] Other muscle resident populations, such as fibroblasts, macrophages, and vascular cell types are also among the major players that have important roles in functional regeneration.[9–12] However, severe traumatic injury and/or congenital or acquired diseases can lead to simultaneous loss of multiple skeletal muscle tissue components, including muscle fibers, nerves, vessels, and extracellular matrix (ECM). When the volume of muscle tissue loss exceeds the capacity of endogenous mechanisms to elicit functional regeneration,[13,14] the injuries are referred to as volumetric muscle loss (VML) injuries. By definition, VML injuries result in permanent functional and cosmetic deficits, usually accompanied by increased fibrosis rather than *de novo* muscle formation.[15]

To date, there is no standard of care for VML injuries that adequately restores form and function.[16] Current treatments for VML injuries frequently involve surgical muscle transfer; these procedures are often associated with poor engraftment and donor-site morbidity. Recently, investigators have described the implantation of an acellular matrix (e.g., urinary bladder matrix, porcine intestinal submucosa) for treatment of VML injuries caused by extremity trauma to the limbs.[17–19] Although these initial findings are encouraging, a relatively modest degree of functional improvement accompanied by limited *de novo* muscle regeneration was reported.[17,18,20] As such, there remains significant room for therapeutic improvement.

Thus, development of new and more effective treatments for VML is an active field of research, which focuses on utilization of different combinations of the three regenerative medicine pillars: biomaterials (scaffolds), bioactive molecules (i.e., growth factors), and cells.[21–26] An impressive number of preclinical therapies have been tested, and recent reviews provide an overview of the field.[27–30] In short, while these studies are instructive, many of them either result in limited *de novo* muscle regrowth, or have not been directly tested in animal models that are biologically translatable or scalable to clinical applications.

Directly relevant to the rationale for the current study is prior work concerning the development of the tissue-engineered muscle repair (TEMR) technology platform. The TEMR technology was designed to enhance endogenous skeletal muscle repair by creating a more favorable microenvironment for regeneration.[31–33] TEMR constructs are created by seeding muscle progenitor cells (MPCs) onto a porcine bladder acellular matrix (BAM) and preconditioning the constructs in a custom-designed, cyclical stretch bioreactor before implantation. This approach has been scaled to test the efficacy of TEMR in progressively larger VML injuries. Specifically, the initial investigations documented functional recovery of 60–70% of contractile force within 2 months of TEMR implantation in an athymic, nude mouse latissimus dorsi (LD) VML injury model ($\approx$20 mg injury). A subsequent study showed a similar degree of functional recovery within 3 months of TEMR implantation in a larger, immunocompetent rat tibialis anterior (TA) VML injury model ($\approx$70 mg injury).[32,33] Most recently, TEMR implantation in an even larger rat LD VML injury model ($\approx$160 mg injury), resulted in $\approx$90% contractile force recovery within 2 months of implantation that was shown to be durable up to 6 months.[34]

The published data are very encouraging, especially with respect to TEMR treatment of sheet-like injuries to the LD muscle. However, despite documented success in the TA VML injury model, our previous work revealed a virtual dichotomy in functional outcomes following TEMR implantation—with less than one-half of the (46%, 6/13) animals displaying significant functional recovery relative to untreated injuries.[32] The working hypothesis advanced from these observations was that the mechanical perturbations (i.e., folding and securing), required to place a sheet-like TEMR construct in the cylindrical geometry of the TA VML injury model, may disrupt TEMR integrity and compromise the biological activity of the implanted construct—resulting in more variable functional outcomes. The goal of the current investigation was to explicitly test this supposition through improved matching of the geometry of the TEMR technology to the TA VML injury environment, and furthermore, to investigate the durability of this treatment effect.

Materials and Methods

Bladder acellular matrix preparation

BAM scaffolds were prepared as previously described.[31–33] Porcine-derived bladder was trimmed to remove excess tissue. Bladders were placed in 0.05% Trypsin with 10 mM ethylenediaminetetraacetic acid (Hyclone, Logan, UT) for 1 h at 37°C, then transferred to Dulbecco's modified Eagle's medium (DMEM; Gibco by Life Technologies, Grand Island, NY) with 10% fetal bovine serum (FBS; Gemini, West Sacramento, CA) and 1% antibiotic/antimycotic (AA; Gibco by Life Technologies) overnight at 4°C. For a subsequent 4 days, bladders were washed in decellularization solution composed of 1% Triton X (Sigma Aldrich, St. Louis, MO) and 0.1% ammonium hydroxide (Fisher Scientific, Pittsburgh, PA) at 4°C. The solution was changed twice per day. The bladders were then washed in deionized water twice each day for 3 days at 4°C. The lamina propria was then peeled from the remaining tissue and cut and draped onto rectangular silicone molds with a 4.5 cm^2 surface area for cell seeding. Scaffolds and molds were placed in cell culture dishes and sterilized by ethylene oxide.

Tissue-engineered muscle repair construct creation

MPCs were isolated from the TA and soleus of 4–6-week-old female Lewis rats (Charles River Laboratories, Wilmington, MA) and seeded onto BAM scaffolds to create the TEMR construct as previously described.[32] Muscles were excised, sterilized in iodine, and cleaned in sequential phosphate-buffered saline (Hyclone) washes. Muscles were hand minced to create a homogenous cell slurry, and then incubated for 2 h at 37°C in 0.2% collagenase (Worthington Biochemicals, Lakewood, NJ) in DMEM. The muscle was then preplated onto 10-cm collagen-coated tissue culture dishes (Corning, Corning, NY) at 37°C in myogenic medium containing DMEM high glucose with 20% FBS, 10% horse serum (Gibco by Life Technologies); 1% chick

embryo extract (Accurate, Westbury, NY), and 1% AA. After 24 h, the cell suspension was transferred to 15-cm Matrigel-coated (1:50; BD Biosciences, Franklin Lakes, NJ) tissue culture dishes. Cells were passaged at 70–90% confluence and further cultured in proliferation media containing DMEM low glucose with 15% FBS and 1% AA.

At passage 3, MPCs were seeded onto both sides of BAM scaffolds at a cell density of 10^6 MPC per cm^2 (5.4 million cells/side). The BAM was tested before seeding to ensure that it was water tight to allow for optimal cell seeding and adherence. The construct was cultured in proliferation media for 3 days, then changed to differentiation media composed of DMEM/F12 (Gibco by Life Technologies) with 2% horse serum and 1% AA for 7 days. Constructs were moved to a cyclic stretch bioreactor and preconditioned with 10% uniaxial strain. Constructs underwent cyclic mechanical stretching as previously described.[31,32,34] In short, their original length at the time of loading was increased by 10% for a total of three times per minute (20 s per stretch) for the first 5 min every hour over the course of 5 days in proliferation media.[31,32] TEMR constructs were implanted immediately upon completion of bioreactor preconditioning.

Creation of the volumetric muscle loss injury

All animals in this study were treated in accordance with the Animal Welfare Act and the Guide for the Care and Use of Laboratory Animals. All procedures were approved by the University of Virginia Animal Care and Use Committee. A total of 26 female Lewis rats (11–14 weeks old with a mean body weight of 198.4 g ± 3.5 g) (Charles River Laboratories) were randomly assigned to treatment groups. Animals were provided with food and water *ad libitum*.

The VML defect was surgically created in the rat TA as previously described.[32,35] A longitudinal incision was made along the lateral side of the left lower hindlimb, from the ankle to the knee. The skin was separated by blunt dissection from the underlying fascia. The fascia was cut and separated from the anterior crural muscles. The extensor digitorum lon (EDL) and extensor hallicus longus (EHL), synergist muscles in the anterior compartment, were isolated and ablated at the tendons to more accurately assess the impact of VML injury and recovery of the TA muscle over time (e.g., avoid compensatory hypertrophy following the injury to the TA).[32] The VML injury was created by excising no <20% of the middle of the TA in an area measuring an area of 1 cm × 0.5 cm × 0.7 cm, and avoiding the underlying tendon (Fig. 1A). The defect size was calculated as 20% of the TA, which was determined experimentally to be 0.17% of the animal's body weight.[32] Immediately post-VML, animals in the no-repair (NR) group ($n = 7$) received no treatment, whereas animals in the BAM group ($n = 7$) and TEMR group ($n = 12$) received a 1 × 2 cm acellular scaffold or cellularized TEMR construct, respectively, which was folded twice (Fig. 1B, C), trimmed at the folded ends to remove excess scaffold, and sutured into the wound bed (6-0 Vicryl; Ethicon, Somerville, NJ) (Fig. 1D). The fascia was also closed with 6-0 vicryl interrupted sutures. The skin was closed with 5-0 prolene (Ethicon) interrupted sutures and skin glue to prevent reopening of the incision. Buprenorphine (0.05 mg/kg) was administered subcutaneously for 3 days postsurgery.

In vivo *function testing*

Functional testing was performed on all animals before VML surgery and/or repair, to establish baseline torque responses for each animal. Posthealing, *in vivo* functional analysis was performed to assess recovery post-VML injury at 8, 12, and 24 weeks. Torque production by the experimental TA was measured *in vivo* as previously described.[32,35,36] Rats were anesthetized (2% isoflurane; Henry Schein, Dublin, OH) and the left hindlimb was aseptically prepared. The rat was placed on a heated platform and the left foot was secured at a 90° angle to a footplate attached to the Aurora Scientific 305C-LR-FP servomotor (Aurora, ON, Canada), controlled by a computer. The left knee was securely clamped and two sterilized percutaneous needle electrodes (Chalgren, Gilroy, CA) were inserted superficially through the skin to stimulate the left peroneal nerve.

An electrical stimulus was applied (Aurora Scientific Stimulator Model 701C) and stimulation voltage and electrode placement were optimized with continuous 1 Hz twitch contractions. Contraction of the anterior crural muscles leading to dorsiflexion of the foot was determined by measuring the maximal isometric tetanic torque over a range of stimulation frequencies sufficient to result in plateau of the torque response (10–150 Hz). At 24 weeks, animals were euthanized through CO_2 inhalation, and injured TA muscles and contralateral control muscles were explanted, weighed, and imaged.

Histological and immunofluorescence analysis

TA muscles were explanted at sacrifice. Excess fascia overlying the experimental muscles was not removed from samples to avoid disturbing the underlying muscle architecture. All tissues were fixed in 4% paraformaldehyde, stored in ethanol, and embedded in paraffin wax. A microtome was used to create 5 μm cross-sections of the experimental and control TA muscles for all animals in each group at 6 months. Hematoxylin and Eosin and Masson's Trichrome stains were performed following standard procedures to assess cellular morphology and fibrosis, respectively.

Images were captured at 4× (Nikon Upright Microscope). The cross-sectional areas of ≈200 muscle fibers in the cortex as well as the core of the TA muscle were manually measured using ImageJ (NIH). The analysis was limited to the most superficial and medial region of the cortex. Specifically, all tissue evaluations were performed on sections obtained within 500 μm from the TA muscle surface, and >1000 μm from the lateral edges of the native muscle. These criteria restricted the tissue analysis safely within the dimensions of the original surgical defect (as highlighted in Figs. 4–8). In the core, measurements were made in a region >1000 μm from the surface of the TA muscle, >500 μm from the bottom of the tissue section, and again, >1000 μm from the lateral edges of the native tissue.

Additional sections were subjected to antigen retrieval (Vector Laboratories; H-3301), autofluorescence reduction protocol (0.3% Sudan Black for 10 min), and overnight blocking at 4°C (Dako Blocking Solution X0909; Agilent Technologies, Santa Clara, CA). Samples were incubated with antibodies against rabbit CD31 (1:250, NB100-2284; Novus Biologicals), mouse smooth muscle actin (SMA) conjugated to Alexa Fluor 488 (1:250, F3777; Sigma-Aldrich), mouse CD68 (1:100, MCA341R; Bio-Rad), rabbit

CD163 (1:400, ab182422; Abcam), chicken neurofilament 200 (NF200, 1:1000; EnCor CPCA-NF-H), mouse myosin heavy chain slow (1:25, BA-F8; DSHB), mouse myosin heavy chain fast (1:25, A4.74; DSHB), and mouse myosin heavy chain type IIB (1:25, BF-F3; DSHB) overnight at 4°C. Secondary antibodies were applied for 2–6 h at room temperature or 4°C using goat α-mouse Alexa Fluor 488 F(ab′)2 fragment (1:500, A11017; Invitrogen), Alexa Fluor 488 goat α-chicken (1:600, A11039; Invitrogen), and Alexa Fluor 594 goat α-rabbit (1:500, A11012; Invitrogen). All antibodies were diluted in Dako Antibody Diluent (Dako Antibody Diluent S0809; Agilent Technologies). Images were captured by confocal microscopy (Leica DMi8; Buffalo Grove, IL). To assess tissue characteristics in the defect/repaired region in a standardized manner, we quantified all markers of interest in a cross-sectional area measuring ~ 525 μm by 935 μm (area of 0.49 mm^2) in the middle of the original defect region, or the comparable region in the control tissue. This approach provided a conservative estimate of tissue that would lay well within the original defect area of the TA; as determined from the calculated cross-sectional area of the original defect in the belly of the TA muscle at day 1 postsurgery (3.05 mm^2, Fig. 1E).

In the 6-month samples that were analyzed in this study, the site of the original VML defect was located by the presence of fibrosis on the surface of the muscle, and in all cases, either an obvious concave depression on the surface of the muscle (e.g., BAM, NR, or nonresponders TEMR), or detectable, albeit sometimes modest disruptions of the normally smooth surface architecture of the surface of the TA muscle. The distinct anatomical structure of the TA due to its close association with the tibia also allowed for ease in determining where the original defect was made. Images from one representative slide per sample, in the same region of the TA muscle for all animals were analyzed for positively stained cells and/or structures as determined by pixel density and recognizable histological hallmarks were manually counted using ImageJ (NIH).

Experimental design

Previous work (both analytical and experimental) demonstrated that 6–8 animals/treatment group provided sufficient power to discriminate biologically relevant statistical differences in contractile force recovery among treatment groups for a similar experimental design. Thus, we originally entered 21 animals in the study (7/treatment group), and when it appeared that we may once again be observing a dichotomy of responses in the TEMR implanted group at the 12-week time point, another five TEMR-treated animals were added to the study. The TEMR-implanted animals were subsequently subdivided into TEMR responder and TEMR nonresponder groups, as described in the results.

Statistical analysis

Unless otherwise stated, data are expressed as mean ± standard error of the mean (SEM). In cases where the data were not normally distributed (nonparametric, as determined by the Shapiro/Wilk Test), data are displayed as the median ± the maximum and minimum values of the data range. Data were analyzed through one- or two-way analysis of variance (ANOVA), as appropriate, with *post-hoc* multiple comparison testing performed when the ANOVA was significant. Statistical significance was assessed at an alpha level <0.05. Analysis was conducted by using GraphPad Prism 8.0 for Windows (La Jolla, CA).

Results

All animals recovered post-VML surgery with no signs of infection and no deaths. A representative example of the TA VML defect 1 day postsurgery is shown in Figure 1E. The body weights of animals in all treatment groups underwent similar increases throughout the duration of the study (Fig. 1F), with a few small, but nonetheless, statistically significant differences in body weight noted among treatment groups (Fig. 1F). All defects had the same dimensions and defect weights were not significantly different between the treatment groups (one-way ANOVA, $p = 0.09$, Fig. 1G).

Evaluation of functional recovery following VML injury and/or repair

There were no significant differences in baseline function values among the four treatment groups (one-way ANOVA, $p = 0.9$, Fig. 2A). Repeated *in vivo* functional testing was performed on each animal at baseline (i.e., before surgery, see section ''Materials and Methods''), as well as 8, 12, and 24 weeks postinjury to assess the physiological status of the TA muscle over time, following VML injury and/or repair. Mean values were expressed as torque normalized to the body weight each time point (Nmm/kg of body weight) to control for increases in torque production due to animal growth (Fig. 2B). Muscle function was also expressed as a ratio of the normalized torque divided by the baseline torque (Fig. 2C) for the same animal at all time points.

As previously reported,[32] our initial observations at 12 weeks indicated the potential for significant variability in TEMR-mediated functional recovery. Therefore, additional animals were added to the study as described in the ''Materials and Methods'' section. At the 6-month time point, this variability was confirmed, so for the purposes of statistical analysis, we subdivided the TEMR-implanted animals into two groups: (i) TEMR responder group defined as all animals with force recovery >64 Nmm/kg, and (ii) TEMR nonresponder group with the remaining animals that had a force recovery of <64 Nmm/kg. Of note, 64 Nmm/kg represents the maximum mean isometric torque in the NR animals and defines the greatest amount of force recovery possible in the absence of any treatment. Based on these criteria, the majority of animals, $n = 8$, were placed in the TEMR responder group, whereas the remaining animals $n = 4$, were placed in the TEMR nonresponder group. These criteria were further reinforced by both gross tissue morphology and tissue histology (Figs. 3 and 4).

A two-way repeated measures ANOVA with the Geissner/Greenhouse sphericity correction was used to evaluate the statistical significance of any changes observed in muscle function during the course of study among the four treatment groups. A significant effect of treatment was detected ($p < 0.0001$), but there was no detectable effect of time ($p = 0.2$), and no treatment-time interaction effect ($p = 0.3$). As shown in Figure 2, Tukey's *post-hoc* testing to determine statistically significant differences among the

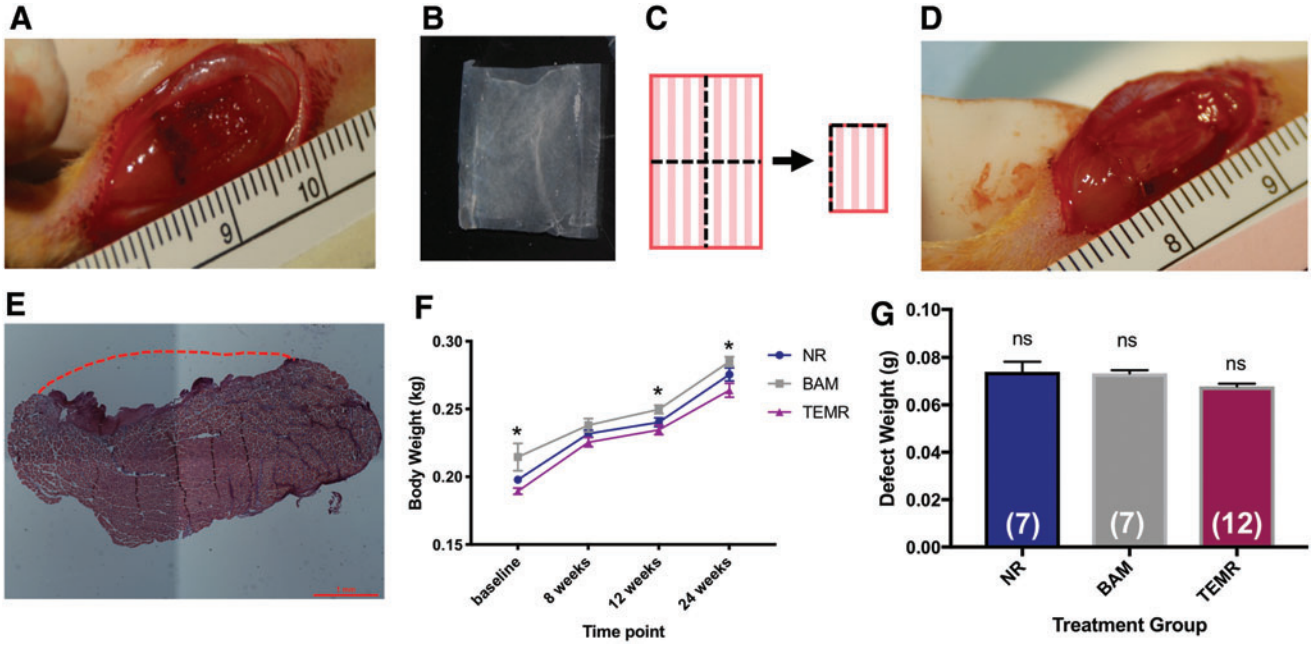

FIG. 1. Creation of a VML injury in the rat tibialis anterior. **(A)** VML injury was created in the middle of the TA muscle measuring $\approx 1\,\text{cm} \times 0.7\,\text{cm} \times 0.5\,\text{cm}$ and weighing no <20% of the TA. **(B)** An unfolded and trimmed TEMR scaffold with uniform cellularity. **(C)** Schematic depiction of TEMR construct folding before implantation. One half of each construct was folded lengthwise, and then in half across the width. **(D)** The folded TEMR construct was carefully placed in the wound bed, sutured, and trimmed to remove excess material. **(E)** H&E staining of the unrepaired TA muscle explanted 1 day post-VML surgery. The *red dashed line* indicates the approximate location of the native muscle preinjury. **(F)** Body weight of the animal during the study. Two-way repeated measures ANOVA revealed an effect of time ($p < 0.0001$), as well as an effect of treatment ($^*p < 0.01$), but no time–treatment interaction. Tukey's multiple comparisons *post-hoc* test indicated a significant difference between NR and TEMR groups body weight at baseline ($^*p < 0.05$) and significant differences between BAM and TEMR group body weight at 12 and 24 weeks ($^*p < 0.05$). **(G)** Weight of excised TA muscle was statistically indistinguishable across all treatment groups. Group sample sizes are listed in *parenthesis*. Values are expressed as the mean ± SEM. SEM, standard error of the mean; ANOVA, analysis of variance; VML, volumetric muscle loss; TEMR, tissue-engineered muscle repair; H&E, Hematoxylin and Eosin; TA, tibialis anterior; NR, no repair; BAM, bladder acellular matrix; ns, not significant. Color images are available online.

treatment groups detected effects at both 8 and 12 weeks. However, the most pronounced effects were detected at 6 months postinjury —where TEMR responders displayed significantly increased functional recovery compared with all other treatment groups (Fig. 2B, C; Table 1).

The statistical conclusions are remarkably similar whether the data are expressed as mean maximal isometric torque (normalized to body weight; Fig. 2B), or as a ratio of the original baseline response on the same animal (Fig. 2C). The statistical analysis documents that the TEMR implantation was not only more effective in increasing the degree of functional recovery in the majority of treated animals, but the response was durable out to 6 months. In addition, we noted that three of the eight TEMR responders (termed TEMR max responders, 38% of TEMR responders, and 25% of all TEMR-implanted animals) were observed to have a functional ratio of 0.74 or above (mean ratio of 0.78 ± 0.02 SEM, recorded maximum isometric torque of 74.3 ± 1.2 Nmm/kg), which represents nearly 90% of the maximum theoretical recovery attainable following synergist ablation in this VML injury model. Note that ablation of the EDL and EHL removes $\approx 20\%$ of torque generation in the anterior compartment, and as such, normalized torque would be limited to ≈ 85 Nmm/kg across the treatment groups.[32]

Gross morphology and histological analysis of tibialis anterior muscles 6 months post VML injury and/or repair

A careful analysis of both gross morphology and histological cross-sections through the belly of the TA muscle was performed (Figs. 3 and 4). Close inspection revealed a convex surface of the explanted experimental TA muscles (Figs. 3D, E, and 4C[v], [vii], and [vii]) as compared with the TA muscles retrieved from the contralateral control leg (Figs. 3F and 4C[i]), which was particularly pronounced in the BAM (Figs. 3D and 4C[v]), NR (Figs. 3E and 4C[vi]), and TEMR nonresponder treatment groups (Fig. 4C[vii]), but more challenging to identify the TEMR responders—in particular the TEMR max responders (Figs. 3A–C and 4C[ii]–[iv]). As further described in the ''Materials and Methods'' section, this convex reference point was used to identify the site of VML injury and/or treatment for retrieved tissue.

The gross morphology and appearance of the TEMR max responders (Figs. 3A–C and 4C[ii]–[iv]) much more closely resembled that of the contralateral control TA muscle (Figs. 3F and 4C[i]), in comparison to the BAM (Figs. 3D and 4C[v]) and NR (Figs. 3E and 4C[vi]) groups. More specifically, in the TA muscle from BAM-implanted

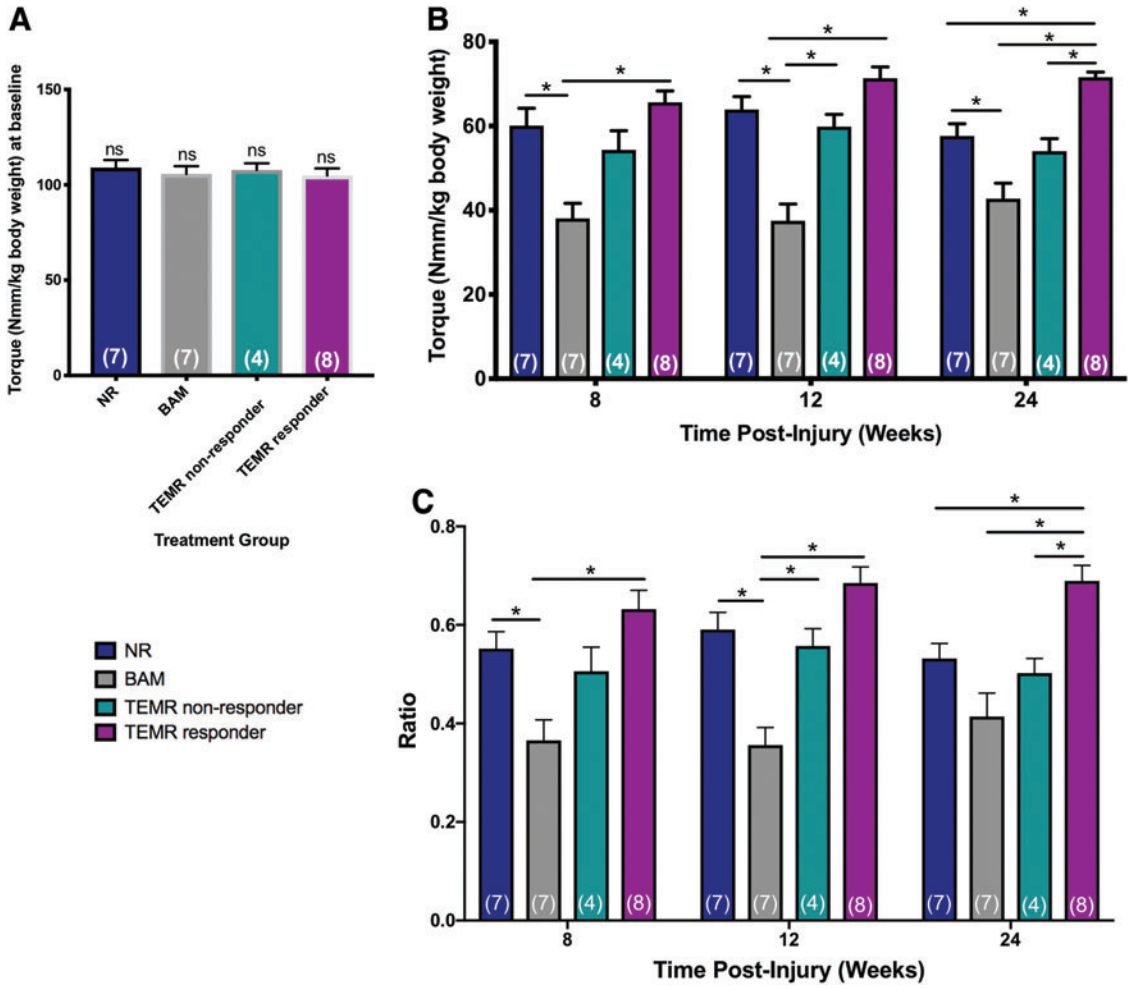

FIG. 2. Analysis of functional recovery of TA muscle contractility in BAM- and TEMR-implanted VML injured rats, as well as VML injured rats that were not repaired (NR). **(A)** Baseline functional measurements performed before VML injury demonstrated equivalent peak isometric tetanic force production by uninjured TA muscles in all four treatment groups (one-way ANOVA $p = 0.8$, ns = not significant). **(B)** Peak isometric tetanic force (Nmm/kg body weight) is shown at each time point and across treatment groups. There are significant treatment effects at each time point (two-way ANOVA for repeated measures with Tukey's *post-hoc* multiple comparisons test, $*p < 0.05$). **(C)** Peak isometric torque presented as a ratio of the individual baseline peak isometric torque on the same animal. A significant effect of treatment was detected at each time point (two-way ANOVA with Tukey's *post-hoc* multiple comparisons test $*p < 0.05$). Group sample sizes are in *parenthesis* and values are expressed as the mean ± SEM. Color images are available online.

animals and the NR group, an obvious depression in the surface of the TA muscle at the site of injury was observed both in the histology and gross morphology of the tissue. Evidence for increased fibrosis was particularly obvious in the TA muscle of the BAM-implanted animals at 6 months. The consistent presence of concavity and/or obvious fibrosis in the BAM-implanted and NR animals, relative to the TEMR and contralateral control TA muscles, provided key hallmarks for analysis of the muscle tissue histology at the site of VML injury and/or implantation.

Assessment of critical tissue characteristics associated with maximal functional recovery following TEMR implantation (i.e., TEMR max responders)

As demonstrated in a recent publication,[34] passive tissue properties (i.e., volume reconstitution *per se*) can provide biomechanical improvements/advantages that result in increased contractile responses in the absence of substantive skeletal muscle regeneration. Given the obvious dichotomy in functional recovery observed in the current report, we sought to evaluate the tissue characteristics associated with long-term maximal functional recovery. To this end, a detailed histological assessment was conducted on the TEMR max responders. The rationale for this focus was to determine how closely the repaired tissue in the TA muscle of the TEMR max responders (best case scenario for functional muscle recovery) recapitulated native muscle tissue architecture and composition at 6 months postimplantation.

Analysis of muscle fiber cross-sectional area

In an effort to better understand the characteristics of the nominally *de novo* regenerated muscle fibers in the area of injury in the TEMR max responders, we quantified the fiber cross-sectional area (FCSA) in the max responder TA muscle

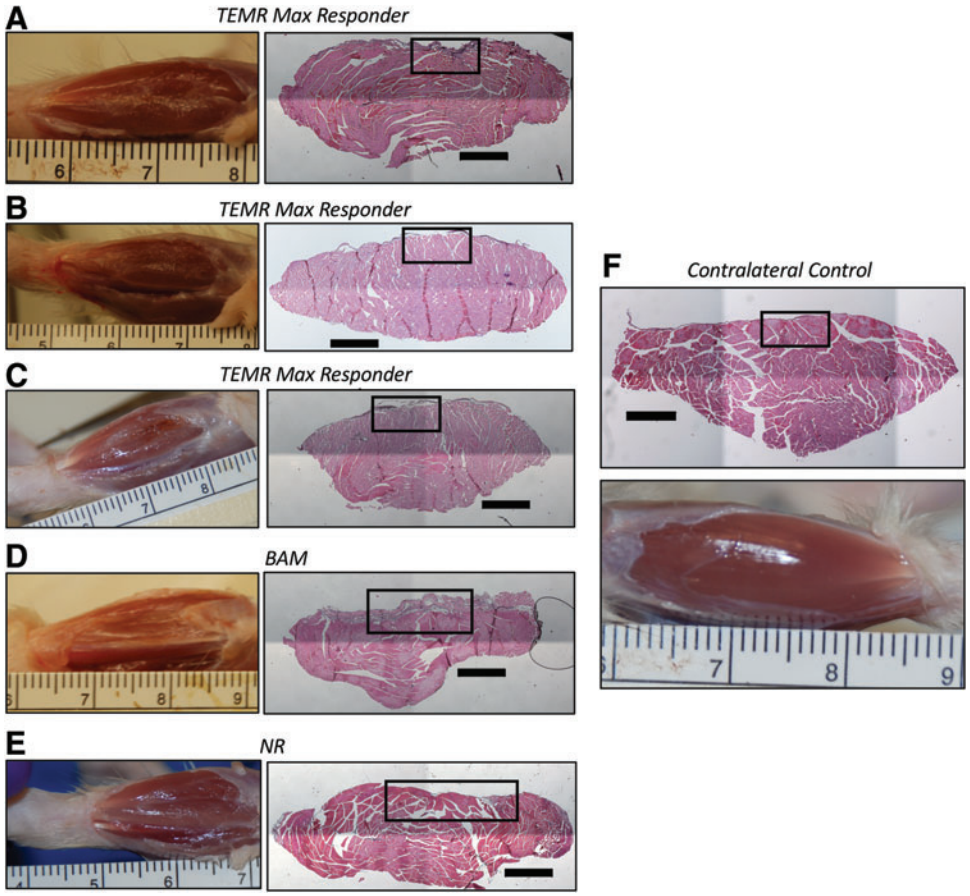

FIG. 3. Gross macroscopic features and histological morphology of the TEMR max responder tissue compared with contralateral control, BAM, and NR muscles. Pictured to *right* of each macroscopic view of the experimental TA muscle is a representative H&E through the belly of the TA muscle—well within the site of the original injury. Representative examples of a TA muscle from the contralateral control leg are also shown. All H&E sections are a region in the middle of the original defect location, <2 mm away from the center of the original defect as identified on the explanted muscle. Defect placement varied slightly due to individual animal anatomy, but sampling was kept as consistent as possible within what was identified as the defect area for each specific muscle. *Black boxes* on the H&E images indicate the region where FCSA was also measured, and those data are shown at higher magnification in Figure 4. All scale bars are 1000 μm. **(A–C)** TEMR max responder muscles. **(D)** BAM-treated muscle. **(E)** NR muscle. **(F)** Contralateral control muscle. FCSA, fiber cross-sectional area. Color images are available online.

and compared it with the same region in the TA muscle of the contralateral control leg. Although as noted above, it was more challenging to detect the region of VML injury and repair than in other treatment groups, the location could still be identified through minor but consistent, microscopic disruptions in the muscle surface architecture and/or the presence of a small band of residual connective tissue (Figs. 3 and 4). Of note, similar FCSA measurements in the BAM-implanted, NR, and TEMR nonresponders are not included because these three latter groups did not have sufficient evidence for, nor a sufficient magnitude of, *de novo* muscle tissue formation to perform this analysis (Figs. 3 and 4). However, a comparative analysis of FCSA on all TEMR responders is included as a Supplementary Figure S1.

The cross-sectional area of ≈ 200 muscle fibers was measured in the area of injury in all three TEMR max responders and compared with the corresponding area of the TA muscle in the contralateral control leg—of those same animals ($n = 3$; Fig. 5). Due to the known heterogeneity in both fiber-type distribution and FCSA in different regions of the TA muscle,[37] great care was taken to ensure that all FCSA measurements were made in the most superficial layers of the TA muscle, referred to as the cortex,[37] or deeper in the middle of the muscle, referred to as the core (see section ''Materials and Methods'' for details) (Fig. 5). Furthermore, all FCSA measurements were made at the center of the defect area in each TA muscle (Fig. 5A). Briefly, measurements made in the original defect area revealed a median FCSA of 849 μm^2 in the cortex for the TEMR max responders, which was slightly, but significantly, smaller than the median FCSA in the cortex of the contralateral control samples (median of 1145 μm^2; Mann–Whitney test, $*p < 0.05$, Fig. 5B). This can be visualized as a slight, but statistically insignificant, leftward shift in the frequency distribution of FCSA in the TA muscle of the TEMR max responders relative to their contralateral control TA muscles (Fig. 5D; multiple *t*-tests correcting for false

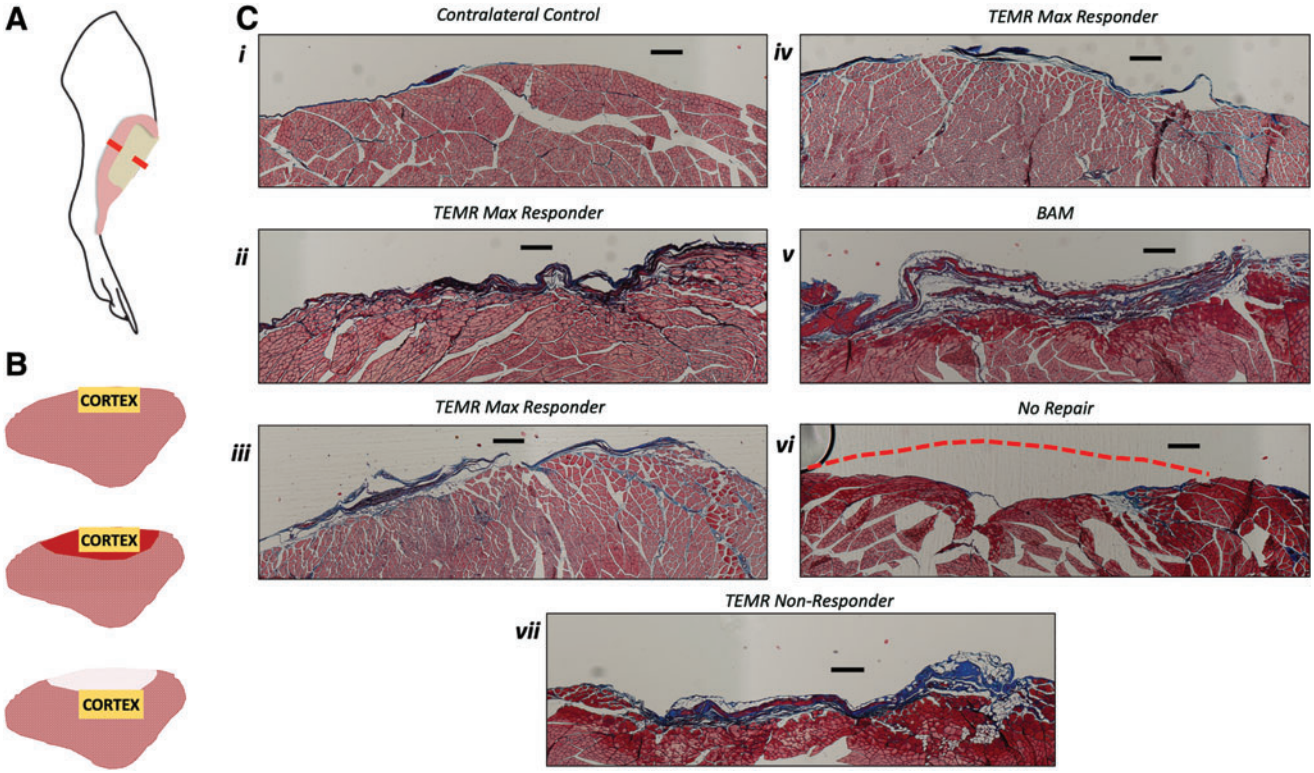

FIG. 4. Representative examples of morphology of the TA cortex in muscles from all treatment groups. **(A)** A schematic illustration of the rat hindlimb demonstrates the location of the TA muscle (*pink area*), placement of the VML defect (*tan area*) and approximate region of the muscle were histological cross-sections were obtained (*red dashed line*). **(B)** Schematic illustration depicting the cortex of TA muscles in the contralateral control leg (*top*), as well as TEMR max responders (*middle*), and TEMR nonresponders, BAM, and NR scenarios (*bottom*). The *yellow box* indicates the region where pictures were obtained in the following panel. In the TEMR max responder (*middle*) muscles, *red shading* indicates the defect region where muscle regeneration occurred. In the BAM and NR (*bottom*) muscles, *white shading* indicates the defect region without new muscle formation. **(C)** Representative examples of the TA muscle where FCSA was measured in the superficial cortex of the TA muscle in the contralateral control leg **(i)**, as well as in TA muscles from the VML injured leg of TEMR max responders **(ii–iv)**, BAM-implanted **(v)** and the most superficial layer of tissue in the NR **(vi)** and TEMR nonresponder **(vii)** animals. *Red dashed lines* indicate where the surface of the muscle appeared concave due to inadequate volume reconstitution during wound healing post-VML. All scale bars are 250 μm. Color images are available online.

discovery rate, $*p > 0.05$). In the core of the TA muscle, the median FCSA of the TEMR max responders (552 μm^2) was also significantly different than the median of the TEMR contralateral controls (680.3 μm^2, Mann–Whitney test, $p = 0.3$, Fig. 5C), although there was no obvious or significant shift in the FCSA frequency distribution (multiple *t*-tests correcting for false discovery rate, $p > 0.05$, Fig. 5E). The range of values measured for FCSA is consistent with what has been previously reported in the literature, although accounting for sex and sampling area differences.[38–40]

Immunofluorescence analysis

To further evaluate the tissue characteristics associated with maximum functional recovery 6 months post-TEMR implantation, we conducted detailed immunofluorescence analyses of retrieved TA muscles from both the TA muscle in the experimental leg of the TEMR max responders ($n = 3$; Figs. 6–8) and the contralateral control leg (see Supplementary Fig. S2 for a representative example). Parallel analyses were also conducted on all of the TEMR responders ($n = 5$; Supplementary Fig. S1).

Evaluation of muscle fiber type

As with the FCSA studies, serial muscle sections for fiber-type analysis were all evaluated in the same region of the superficial cortex and in the deeper core section of the TA muscle, with the core representing an area remote from the site of the original VML defect and repair (Fig. 6A). In the cortex, two-way ANOVA revealed no effect of treatment ($p > 0.9$), and no treatment–fiber-type interaction ($p > 0.9$), but a significant effect of fiber type ($p < 0.05$). In the core, two-way ANOVA also revealed no effect of treatment ($p > 0.9$), but in contrast, no effect of fiber type either ($p = 0.08$). Taken together, the lack of treatment effect between the TEMR responders and contralateral controls suggests that when maximal functional recovery following TEMR implantation is observed, it is associated with restoration of native muscle fiber composition in the injured area.

Evaluation of vascularization and neuronal innervation

Vascularization of the original defect area was also evaluated (Fig. 7A). Capillaries were counted and analyzed separately from larger vessels. Capillaries were identified as

Table 1. Tibialis Anterior Muscle *In Vivo* Functional Capacity and Explant Weights

	Contralateral control	*No repair (NR)*			*BAM*			
Sample size (n)	26	7			7			
Muscle weight at explant (g)	463 ± 4.75	372 ± 11.7*			353 ± 12.6*			
Time point (weeks)		*Baseline*	*8*	*12*	*24*	*Baseline*	*8*	*12*	*24*
P_0 (Nmm/kg)	—	109.1 ± 0.1	60.1 ± 4.1	63.9 ± 3.1	57.6 ± 2.9	105 ± 4.1	38.1 ± 3.6	37.5 ± 4	42.7 ± 3.7
Force ratio	—	—	0.55 ± 0.04	0.59 ± 0.04	0.53 ± 0.03	—	0.36 ± 0.04	0.36 ± 0.04	0.41 ± 0.05

	TEMR nonresponder				*TEMR responder*			
Sample size (n)	4				8			
Muscle weight at explant (g)	368 ± 14.2*				388 ± 7.5*			
Time point (weeks)	*Baseline*	*8*	*12*	*24*	*Baseline*	*8*	*12*	*24*
P_0 (Nmm/kg)	108 ± 3.4	54.3 ± 4.3	59.9 ± 2.9	54 ± 3	105 ± 3.6	65.6 ± 2.7	71.4 ± 2.7	71.6 ± 1.3
Force ratio	—	0.51 ± 0.05	0.56 ± 0.04	0.50 ± 0.03	—	0.63 ± 0.04	0.69 ± 0.03	0.69 ± 0.03

All data are represented as the mean ± SEM. Significant differences compared with contralateral control muscles (*$p < 0.05$) are indicated. P_0 is peak isometric torque (Nmm/kg body weight). Force ratio is represented as the peak isometric torque at the time point normalized to the peak isometric torque at baseline. Graphical results with statistical significance are shown in Figure 2.

SEM, standard error of the mean; TEMR, tissue-engineered muscle repair; BAM, bladder acellular matrix.

vessels <10 μm diameter that were $CD31^+$ and had no distinctive band of smooth muscle (α-SMA^-). All other vessels were defined as having a diameter >10 μm and were positive for CD31 as well as α-SMA, with a progressively increasing α-SMA^+ layer (Fig. 7B). There were no significant differences in the number of capillaries or vessels in the original defect area in the TEMR max responder group compared with TEMR contralateral controls (Mann–Whitney test, $p = 0.18$ for capillaries and $p = 0.051$ for vessels, Fig. 7C, D).

Innervation is also a prerequisite for healthy and functional muscle,[41] thus reinnervation of the *de novo* regenerated muscle tissue in the TEMR max responder group was quantified. We measured the amount of NF200 staining in the original defect area (Fig. 7E, F).[22] There was no significant difference in the extent of NF200 staining between the TEMR max responder and contralateral control muscles (t-test, $p = 0.7$, Fig. 7F).

Evaluation of macrophage response

The macrophage response following VML injury is critical for a positive regenerative outcome. Therefore, we assessed the total macrophage presence in the defect area using CD68 and CD163 staining in the TA muscle of the three TEMR max responders, as well as the pooled values from the TA muscle in the contralateral control leg. We observed an elevated, but nonstatistically significant (Mann–Whitney test, $p = 0.1$) number of $CD68^+/CD163^-$ macrophages as well as $CD68^+/CD163^+$ macrophages (Mann–Whitney test, $p = 0.09$) in the TEMR max responders (Fig. 8), indicative of a chronic remodeling response.[42,43]

Comparison of TEMR max responders and TEMR responders

As noted above, we also conducted parallel analyses on the rest of the TEMR responders ($n = 5$) as well. Importantly, a comparison of the TEMR max responders with the rest of the TEMR responders revealed significant differences in only the median FCSA values (Supplementary Fig. S1). Otherwise, these initial investigations indicate that over a range of submaximal functional recovery values (66.5–76.6 Nmm/kg), there were no significant differences detected in fiber type, fiber distribution, vascularization, or innervation between the TEMR max responders and TEMR responders.

Discussion

Scarless wound healing with complete functional recovery is the ultimate goal of tissue engineering and regenerative medicine approaches to VML injury. Unfortunately, in studies where functional outcomes were rigorously documented, most VML repair technologies are associated with increased contractile force in the presence of only low, partial, or modest regeneration of skeletal muscle.[15,21,35,38,44–47] In fact, there are a variety of biomechanical mechanisms that can contribute to increased contractile force post-VML injury despite limited skeletal muscle regeneration.[2,34,38,48] In particular, volume reconstitution *per se*, has a major impact on passive tissue properties,[34] thus improving contractile force by providing a connective tissue bridge between damaged segments of skeletal muscle. At the optimal muscle length, this bridge can accommodate improved muscle fiber shortening and enhanced contraction in the presence of minimal muscle regeneration.

Over the past several years, we have published a series of articles in progressively larger rodent VML injury models (ranging from a ≈25 to 160 mg muscle tissue defect) demonstrating that within 3 months of TEMR transplantation, in both immunocompetent and incompetent animals, 60–90% functional recovery is observed in the presence of demonstrable and reproducible (albeit sometimes modest) levels of muscle fiber regeneration inside the transplanted construct region. These findings bode well for potential future clinical applications of this technology platform, especially with respect to some of the smaller muscles of the face (e.g.,

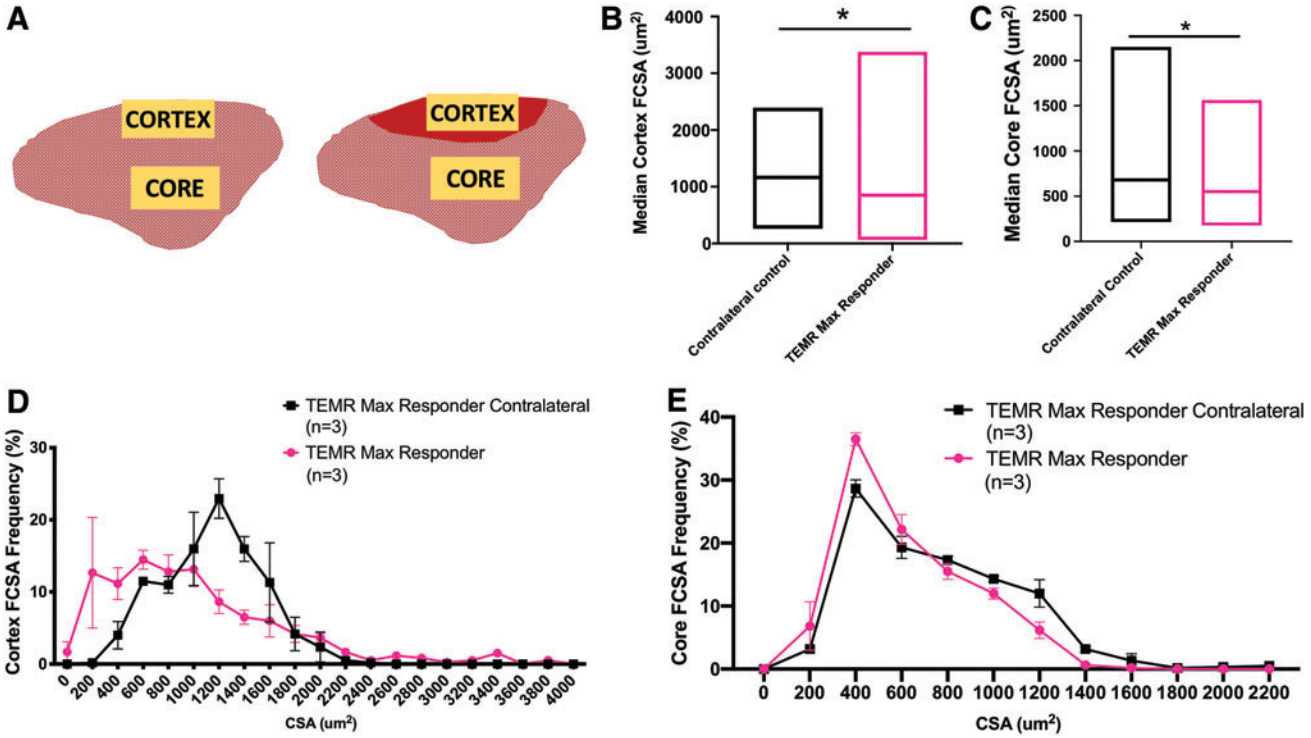

FIG. 5. Comparison of FCSA in TA muscles retrieved from TEMR max responders and contralateral control legs. **(A)** Schematic representation of the contralateral (*left*) and TEMR max responder (*right*) rat TA muscle. *Yellow boxes* indicate regions of the cortex and core where measurements were obtained. *Red shading* on the TEMR responder indicates the defect area where *de novo* muscle regeneration nominally occurred. **(B)** Median FCSA measurements were calculated from ~200 fibers in the cortex of the TA from each animal (TEMR max responder contralateral $n=3$, TEMR max responder $n=3$). Medians were significantly different ($^*p<0.05$, Mann–Whitney test) from each other. Values are the shown as the median with minimum to maximum range due to the nonparametric distribution of the data. **(C)** Median FCSA measurements were calculated from ~200 fibers in the core of the TA from each animal (TEMR max responder contralateral $n=3$, TEMR max responder $n=3$). Medians were significantly different ($^*p<0.05$; Mann–Whitney test) from each other. Values are shown as the median with minimum to maximum range. **(D)** The TEMR max responder cortex FCSA frequency distribution curve displays a similar range of FCSA values as that of the contralateral muscles, with no significant differences in any bin size (multiple *t*-tests correcting for false discovery rate, $p>0.05$ at all points). **(E)** The TEMR max responder core FCSA frequency distribution curve displays a similar range of FCSA values as that of the contralateral muscles, and there were no significant differences in any bin size (multiple *t*-tests, $p>0.05$ at all points). Please note that when grouped into bins, FCSA had a normal distribution, and therefore, parametric statistical analyses were used. Whereas analysis of the entire population of FCSA values revealed a non-normal distribution and required nonparametric statistical analyses. Color images are available online.

orbicularis oris) and hand (e.g., adductor pollicis) that scale well to recent findings in the rodent LD model.[34]

Nonetheless, there is still room for therapeutic improvement and observations to date indicate that the TEMR technology may be better suited for more sheet-like VML injuries (e.g., LD muscle), with more favorable geometries. The goal of the present study was to test the ability of the TEMR to promote functional recovery in an injury that was better suited to the dimensions of the construct. This would determine if improved matching of TEMR geometries within the injury site could mitigate the previously noted virtual dichotomy in functional recovery. Thus, great care was taken in the presurgical handling and implantation of the TEMR constructs. In addition, although the TEMR constructs in both studies were produced using an identical manufacturing process,[34] the dimensions of the constructs from our prior work [1.5 cm × 4 cm; (32)] were different than those used in the current study (2.7 cm × 2 cm), as were the dimensions of the VML injury into which they were implanted; most specifically with respect to the width of the injury ≈0.7 cm in the current study compared with ≈0.5 cm in our prior work.[32]

As shown in Figure 1, taken together, these modifications provided an improved fit of the TEMR construct at the site of the VML injury. Also shown in Figure 1, despite these changes, the amount of tissue removed when creating the TA VML injury, as well as the magnitude of the functional deficit that resulted from that injury, were virtually identical to our prior report,[32] confirming that the changes we made to the geometry of the injury did not change the nature of the injury. However, in addition to the modifications to the injury dimensions, we also significantly adjusted the design of the TEMR construct by changing the size and folding patterns. This resulted in a thinner construct that directly matched the shallower void of the injury relative to our prior report.[32]

However, despite these adjustments, there was again noteworthy variability in the degree of functional recovery following TEMR implantation in the rat TA VML injury model. In fact, the degree of functional recovery ranged from zero in the four TEMR nonresponders (Table 1) to near the theoretical maximum functional recovery possible in the three TEMR max responders (see below).

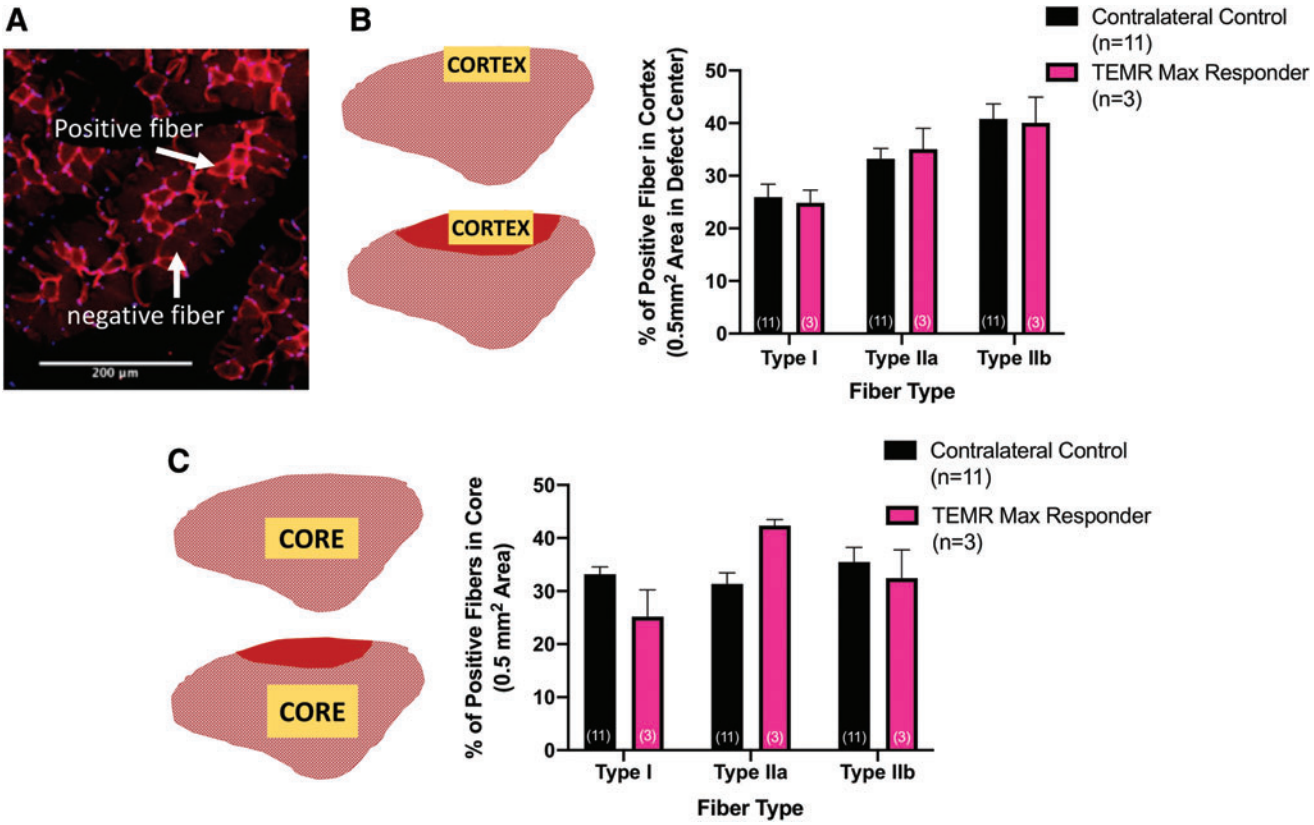

FIG. 6. Fiber-type analysis of TEMR max responders compared with contralateral controls. **(A)** Representative staining in the TA core demonstrating the evaluation of positive and negative fibers for each of the three fiber types assessed. **(B)** Fiber-type quantification in the cortex of the contralateral control TA muscle of TEMR-implanted animals (*top* schematic) as well as in the wound region of the experimental TA muscle of TEMR max responders (*bottom* schematic). In the cortex, two-way ANOVA revealed no effect of treatment ($p > 0.9$), and no treatment–fiber-type interaction ($p > 0.9$), but a significant effect of fiber type ($p < 0.05$). **(C)** In the core, two-way ANOVA also revealed no effect of treatment ($p > 0.9$), and no interaction ($p > 0.9$), but in contrast, no effect of fiber type either ($p = 0.08$). In both graphs, values are the mean ± SEM and sample sizes (n) are in *parentheses*. In all cases, *yellow shaded* regions on the muscle schematics denote area from which measurements were obtained. *Red shading* indicates the defect area with improved muscle tissue formation. One contralateral control sample was excluded from analysis due to poor fiber-type staining quality. Scale bar is equal to 200 µm. Color images are available online.

The major findings of this study are as follows, and will be discussed in more detail: (i) In stark contrast to previous observations where functional recovery was observed in only 46% of TEMR-implanted animals (6/13 animals) at 12 weeks post-VML injury, in the current study, 67% of TEMR-implanted animals (8/12) displayed significantly greater peak isometric torque than all other treatment groups at 6 months post-VML injury; (ii) 3/8 ($\approx$38%) of the TEMR responders, denoted as the TEMR max responders, recovered to the near theoretical maximum possible level of force production ($\approx$85 Nmm/kg); (iii) Close inspection of the macroscopic and microscopic tissue properties of the TEMR max responders documented that the TEMR-implant region was associated with *de novo* muscle tissue formation that closely approximated the characteristics and architecture of native skeletal muscle; and (iv) Analysis of the remaining TEMR responders ($n = 5$; 62%) revealed that over a range of submaximal functional recovery values (66.5–73.9 Nmm/kg) there were also no significant differences detected in fiber type, fiber distribution, vascularization, or innervation when compared with the TEMR max responders.

There are a few potential mechanisms by which we hypothesize that the changes to the implantation strategy enhanced functional outcomes following TEMR implantation. The shallower injury resulted in more uniform and undisturbed layers of the TEMR construct (i.e., no mechanical deformations of the scaffold resulting from geometry mismatch), as well as a cleaner interface with the native tissue (Fig. 1A–D). This, in turn, may have allowed for increased cell migration and nutrient flow, which presumably, would enhance remodeling of the defect area, and presumptively improved regeneration. That is, because the TEMR construct fit optimally into the VML defect, there was less mechanical disruption during implantation, thus maintaining the biological integrity of the cells on the scaffold. Further work will be required to shed additional light on the precise mechanisms responsible for the improved TEMR-mediated functional regeneration observed herein.

Increased frequency of TEMR responders

The frequency of the TEMR responders increased by nearly 50% in the current study (from 6/13 to 8/12), accounting for 67% of the total TEMR-implanted population. However, it is important to note that the first study was terminated at the 12-week time point, whereas this study continued until the 6-month time point. Moreover, the

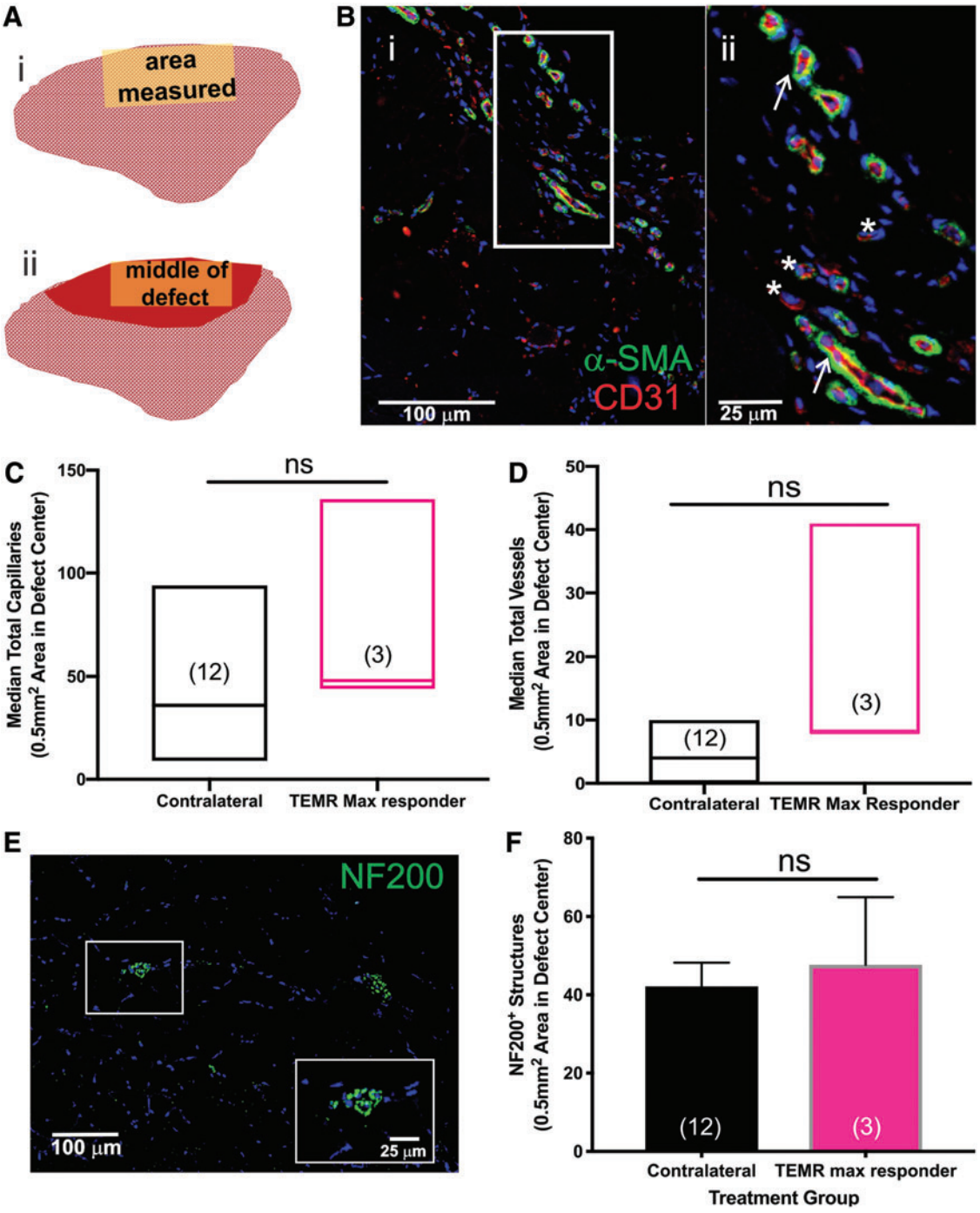

FIG. 7. Comparison of vasculature and neuronal innervation in the TA muscle of the TEMR max responders. **(A)** Cross-sectional schematic of the TA indicating where IF measurements were made in the contralateral control muscles **(A[i])**, and in the TEMR max responder muscles **(A[ii])**. *Red shading* indicates the region in the cortex where nominal *de novo* muscle regeneration was observed at the site of the original defect. Representative capillary and vessel staining in the **(B[i])** representative TEMR max responder TA. Sections were stained for α-SMA (smooth muscle cells) and CD31 (endothelial cells) and the number of capillaries (*white asterisks*) and vessels (*white arrows*) were manually counted in the same region of interest in each sample, as described in the section ''Materials and Methods.'' Representative staining is shown in a higher magnification *inset* **(B[ii])** that corresponds to the outlined area shown in **(B[i])**. **(C)** Capillaries and **(D)** vessels were quantified. There were no statistically significant differences between TEMR max responders and the contralateral control TA muscles ($p > 0.05$, Mann–Whitney test). Because the data were not normally distributed, the values are expressed as the median ± range; sample sizes are in *parentheses*. **(E)** Representative neuron staining in the rat TEMR max responder muscle. *Punctate dots* were counted as occurrences of positive staining. The *inset* shows a higher magnification of NF200 staining. **(F)** TEMR max responders had levels of innervation comparable to the native contralateral controls (by unpaired *t*-test, ns = not significant, $p = 0.7$). Values are expressed as the mean ± SEM; sample sizes are in *parentheses*. IF, immunofluorescence; SMA, smooth muscle actin. Color images are available online.

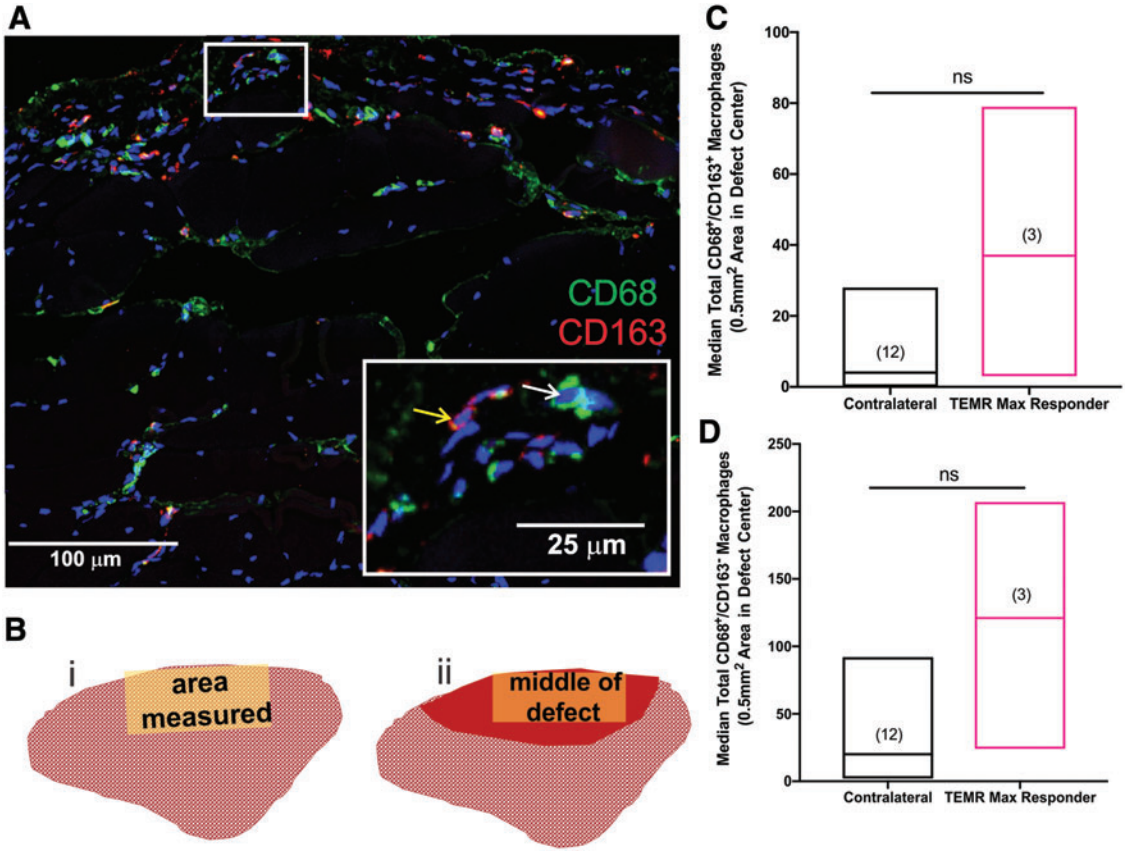

FIG. 8. Analysis of macrophage staining in TA muscles from the contralateral control leg and TEMR max responders. **(A)** Representative macrophage staining in TA muscle from a TEMR max responder. $CD68^+$ (*inset*, *white arrow*) and $CD163^+$ (*inset*, *yellow arrow*) macrophages can be observed 24 weeks post-TEMR implantation. The *white box* is shown at a higher magnification in the *inset*. **(B)** Cross-sectional schematic of the TA muscle indicating where IF measurements were made in the TA muscles from contralateral control legs **(B[i])** and the implanted leg of the TEMR max responder **(B[ii])**. *Red shading* indicates the region in the cortex where nominal *de novo* muscle regeneration was observed in the site of the original defect. **(C)** Although $CD68^+/CD163^+$ macrophage numbers appeared elevated in the TEMR-implanted region, they were not significantly different (by Mann–Whitney test, ns = not significant; $p = 0.1$) from the staining observed in the TA muscle from the contralateral control leg. **(D)** $CD68^+/CD163^-$ macrophage numbers appeared elevated in the TEMR-implanted region, although not significantly different (Mann–Whitney test, ns = not significant; $p = 0.09$). Values are expressed as the median ± range; sample sizes are noted in *parentheses*. Color images are available online.

functional recovery observed in this report was not statistically significant until the 6-month time point. The precise reason(s) for the time differential in functional recovery between the two studies are not known and require further investigation, but previous work suggests that remodeling is a dynamic process that occurs throughout the postinjury timeline.[38] Clearly, an improvement in frequency as well as durability out to 6 months, which is a very significant fraction of the rat lifetime, can still be considered as important steps in the positive direction.

Nearly 40% of the TEMR-implanted animals had functional recovery that was near the theoretical maximum possible levels of torque

The EDL and EHL muscles from the anterior compartment were ablated at the time of creation of the VML injury in the TA muscle. Our previous work has shown[32] that this results in a permanent ≈20% reduction in the peak torque response generated by stimulation of the peroneal nerve. In this scenario, which removes any effects of compensatory synergist action or hypertrophy and allows for mechanistic studies of the impact of VML injury and repair solely on the TA muscle, the peak torque response could be no greater than ≈85 Nmm/kg body weight. Thus, the mean peak torque response of the TEMR max responders of ≈74 Nmm/kg body weight represents a functional recovery of ~87% of the theoretical maximum response possible, whereas the maximum value detected of 76.6 Nmm/kg is an ≈90% force recovery.

TEMR max responders display macroscopic and microscopic features that closely approximate native muscle characteristics and architecture

This observation is also in stark contrast to our previous report. While there was an overall shift to a slightly smaller median FCSA in the TEMR max responders relative to the contralateral controls, the range of FCSA values detected in the TEMR max responders is still representative of that

found in the contralateral control leg, or native TA muscle from those same animals (Fig. 5). In addition, the fiber-type distribution in the repaired region of the TEMR max responders (superficial cortex) was statistically indistinguishable from that of the contralateral control TA muscle (Fig. 6). The relative proportion of fiber types that we observed, specifically Type I, is larger than reported in the literature for the superficial levels of the TA.[40,49,50] Here, that might be attributable to differences in sampling techniques as well as variation in sampling areas within the TA muscle as compared to other studies. Moreover, as noted above, this finding of increased Type I fibers in the cortex may reflect the dynamic remodeling process over time—a possibility that is consistent with the proportion of smaller fiber sizes found in the TEMR max responders.

The observation that NF200 staining was indistinguishable between the TA muscles of the contralateral control legs and the TEMR-implanted TA of the TEMR max responders (Fig. 7) provides evidence for re-establishment of normal innervation patterns at 6 months post-VML injury and is consistent with the fact that muscle volume and the peak isometric torque in this treatment group approached the theoretical maximum response possible. Although not shown herein, we observed no evidence of fiber-type clumping. This is relevant, as fiber-type clumping can be one indication of potentially aberrant reinnervation following TA regeneration/repair. Taken together, the absence of obvious clumping in the TA muscle of the TEMR max responders (or the contralateral controls), in conjunction with the equivalent NF200 staining in the same two groups, would suggest that nominally normal reinnervation patterns were re-established at the 6-month time point.[49]

Finally, quantification of capillary number/density (vessels $<10\,\mu m$) as well as the number of larger vessels ($>10\,\mu m$) demonstrated that the vascularization of the TA muscle of the TEMR max responders was indistinguishable from that of the contralateral control TA muscle. Thus, TEMR-implantation in the max responders may promote angiogenesis to near-native levels. Although angiogenesis alone is insufficient for functional recovery of injured muscle,[24,51] clearly this finding provides additional evidence consistent with a TEMR-mediated repair of VML injury to native-like muscle characteristics, with near-complete force recovery as well. Although this is the most complete regenerative response we have observed to date, the sample size ($n=3$) for the TEMR max responders is still relatively small, and thus, future investigations are expected to yield additional mechanistic insight into the biomimetic potential of this technology in this VML injury model.

Macrophage involvement in continuous remodeling?

Finally, it is important to point out that we are studying the macrophage response at 24 weeks postsurgery. Typically, the macrophage response that occurs in the first 14 days or so following skeletal muscle injury,[43,52–54] is critical to the regenerative success of tissue repair following muscle injury, so measuring the presence of macrophages at 24 weeks post-VML injury is not indicative of the inflammatory response that occurred in the initial muscle repair period. Nonetheless, macrophage activity is important for positive regenerative outcomes as macrophages are known to drive the degradation of implanted scaffolds and this response following treatment can be modulated by various scaffold materials.[43,55–57] Thus, another strength of this study is the quantification of immune cells in repaired muscle with well-documented functional outcomes. This permits a preliminary comparison of macrophage presence in such experimental tissue to the native muscle resident macrophage population in the TA muscle of the contralateral control leg.[58,59] In this regard, we did not observe significantly different numbers of macrophages between the contralateral and TEMR max responder TA muscles, which at this time point may reflect a trend towards stabilization of the remodeling response. As noted above, the sample size ($n=3$) for the TEMR max responders is still relatively small, thus, despite the exciting implications of this initial finding, future studies will further inform the mechanistic basis for our current conclusions.

TEMR implantation is associated with native-like tissue properties over a range of values of functional recovery

Although these initial studies revealed significant differences in median FCSA between the TEMR max responders ($n=3$) and the rest of the TEMR responders ($n=5$), there were no differences in the overall distribution of the FCSA values between these groups, and moreover, immunohistochemical analysis revealed that over the range of submaximal functional recovery values (66.5–76.5 Nmm/kg) there were no significant differences detected in fiber type, fiber distribution, vascularization, or innervation.

The importance of inclusion of a cellular component

We did not observe an increase in force production or muscle fiber regeneration following BAM treatment as previously reported.[32] In fact, both the TEMR responders and TEMR nonresponders, as well as the NR animals displayed significantly greater degrees of functional recovery when compared with BAM throughout the duration of the investigation. This stands in contrast to our previous report,[32] where BAM implantation was associated with a significant functional recovery beyond that observed with NR at 12 weeks—although the TEMR responders in that same study still displayed significantly great torque than BAM (2.3-fold). The precise reason for this discrepancy in the efficacy of BAM implantation is not clear, although it is possible that the decreased amount of total ECM delivered in these studies, due to the changes in scaffold folding reduced the volume of BAM-mediated tissue reconstitution, thus altering the contribution of the passive tissue component to force recovery. This study further reinforces the importance of including a cellular component during implantation of a decellularized ECM to obtain more reproducible and robust degrees of functional recovery in this biologically relevant rat TA VML injury model.

Conclusions

The present study is a logical continuation of prior work and confirms and extends many of those original findings. The current report documents that improved fit, created by modifying the alignment and geometry of the TEMR

construct to better match the surgically created VML injury at the time of implantation improves the observed degree of functional recovery and native-like tissue reconstitution. Presumably, this is attributable to lower levels of mechanical disruption and improved three-dimensional fit of the TEMR construct in the site of the TA VML injury.

Overall, this approach results in ≈50% increase in the frequency of observing statistically significant functional recovery. Moreover, the mean magnitude of functional recovery observed at 6 months in this study is equivalent to that observed at 12 weeks in the prior report, and therefore appears quite durable over a large fraction of the rodent lifespan. Perhaps most importantly, TEMR implantation in the TEMR max responders (≈38% of all TEMR responders) is accompanied by a degree of skeletal muscle repair that approximates that of native skeletal muscle with respect to tissue volume, peak isometric torque, FCSA, and fiber-type distribution, as well as normalization of vascularization and innervation. The remaining 62% of TEMR responders also displayed native-like skeletal muscle tissue properties that were largely indistinguishable from the TEMR max responders over a range of functional recovery values. While further improvements are clearly required, these observations highlight the importance of iterative improvements to the TEMR technology platform in the pursuit of a broader range of potential clinical applications, with increased functional outcomes, for the treatment of VML injuries.

Acknowledgments

The authors would like to thank Dr. Bruna Farjun, Sarah Dyer, and Kim Smith for their assistance in developing analysis techniques, Jack Dienes for his help with muscle explants, as well as Dr. Wendy Novicoff, PhD, Professor, Department of Public Health Sciences and Orthopedic Surgery, for her guidance on the statistical analysis of data.

Disclosure Statement

No competing financial interests exist.

Funding Information

This work was supported by the United States Army Medical Research and Materiel Command/United States Army Medical Research Acquisition Activity (W81XWH-15-2-0012) and E.L.M. was supported in part by the UVA Pharmacology Training Grant (T32 GM007055) and the University of Virginia Wagner Fellowship.

Supplementary Material

Supplementary Figure S1
Supplementary Figure S2

References

1. Jarvinen, T.A., Jarvinen, T.L., Kaariainen, M., Kalimo, H., and Jarvinen, M. Muscle injuries: biology and treatment. Am J Sports Med **33,** 745, 2005.
2. Greising, S.M., Dearth, C.L., and Corona, B.T. Regenerative and rehabilitative medicine: a necessary synergy for functional recovery from volumetric muscle loss injury. Cells Tissues Organs **202,** 237, 2016.
3. Corona, B.T., Wenke, J.C., and Ward, C.L. Pathophysiology of volumetric muscle loss injury. Cells Tissues Organs **202,** 180, 2016.
4. Ciciliot, S., and Schiaffino, S. Regeneration of mammalian skeletal muscle. Basic mechanisms and clinical implications. Curr Pharm Des **16,** 906, 2010.
5. Mauro, A. Satellite cell of skeletal muscle fibers. J Biophys Biochem Cytol **9,** 493, 1961.
6. Scharner, J., and Zammit, P.S. The muscle satellite cell at 50: the formative years. Skelet Muscle **1,** 28, 2011.
7. Zammit, P.S., Partridge, T.A., and Yablonka-Reuveni, Z. The skeletal muscle satellite cell: the stem cell that came in from the cold. J Histochem Cytochem **54,** 1177, 2006.
8. Lepper, C., Partridge, T.A., and Fan, C.M. An absolute requirement for Pax7-positive satellite cells in acute injury-induced skeletal muscle regeneration. Development **138,** 3639, 2011.
9. Murphy, M.M., Lawson, J.A., Mathew, S.J., Hutcheson, D.A., and Kardon, G. Satellite cells, connective tissue fibroblasts and their interactions are crucial for muscle regeneration. Development **138,** 3625, 2011.
10. Kostallari, E., Baba-Amer, Y., Alonso-Martin, S., *et al.* Pericytes in the myovascular niche promote post-natal myofiber growth and satellite cell quiescence. Development **142,** 1242, 2015.
11. Chazaud, B., Sonnet, C., Lafuste, P., *et al.* Satellite cells attract monocytes and use macrophages as a support to escape apoptosis and enhance muscle growth. J Cell Biol **163,** 1133, 2003.
12. Christov, C., Chretien, F., Abou-Khalil, R., *et al.* Muscle satellite cells and endothelial cells: close neighbors and privileged partners. Mol Biol Cell **18,** 1397, 2007.
13. Grogan, B.F., and Hsu, J.R. Skeletal trauma research, C. Volumetric muscle loss. J Am Acad Orthop Surg **19 Suppl 1,** S35, 2011.
14. Garg, K., Ward, C.L., Hurtgen, B.J., *et al.* Volumetric muscle loss: persistent functional deficits beyond frank loss of tissue. J Orthop Res **33,** 40, 2015.
15. Garg, K., Corona, B.T., and Walters, T.J. Therapeutic strategies for preventing skeletal muscle fibrosis after injury. Front Pharmacol **6,** 87, 2015.
16. Lawson, R., and Levin, L.S. Principles of free tissue transfer in orthopaedic practice. J Am Acad Orthop Surg **15,** 290, 2007.
17. Mase, V.J., Jr., Hsu, J.R., Wolf, S.E., *et al.* Clinical application of an acellular biologic scaffold for surgical repair of a large, traumatic quadriceps femoris muscle defect. Orthopedics **33,** 511, 2010.
18. Han, N., Yabroudi, M.A., Stearns-Reider, K., *et al.* Electrodiagnostic evaluation of individuals implanted with extracellular matrix for the treatment of volumetric muscle injury: case series. Phys Ther **96,** 540, 2016.
19. Sicari, B.M., Rubin, J.P., Dearth, C.L., *et al.* An acellular biologic scaffold promotes skeletal muscle formation in mice and humans with volumetric muscle loss. Sci Transl Med **6,** 234ra58, 2014.
20. Sicari, B., Dearth, C.L., and Badylak, S.F. Tissue engineering and regenerative medicine approaches to enhance the functional response to skeletal muscle injury. Anat Rec (Hoboken) **297,** 57, 2014.
21. Quarta, M., Cromie, M., Chacon, R., *et al.* Bioengineered constructs combined with exercise enhance stem cell-mediated treatment of volumetric muscle loss. Nat Commun **8,** 15613, 2017.

22. Kim, J.H., Ko, I.K., Atala, A., and Yoo, J.J. Progressive muscle cell delivery as a solution for volumetric muscle defect repair. Sci Rep **6,** 38754, 2016.
23. VanDusen, K.W., Syverud, B.C., Williams, M.L., Lee, J.D., and Larkin, L.M. Engineered skeletal muscle units for repair of volumetric muscle loss in the tibialis anterior muscle of a rat. Tissue Eng Part A **20,** 2920, 2014.
24. Li, M.T., Ruehle, M.A., Stevens, H.Y., *et al.* Skeletal myoblast-seeded vascularized tissue scaffolds in the treatment of a large volumetric muscle defect in the rat biceps femoris muscle. Tissue Eng Part A **23,** 989, 2017.
25. Matthias, N., Hunt, S.D., Wu, J., *et al.* Volumetric muscle loss injury repair using in situ fibrin gel cast seeded with muscle-derived stem cells (MDSCs). Stem Cell Res **27,** 65, 2018.
26. Qazi, T.H., Mooney, D.J., Pumberger, M., Geissler, S., and Duda, G.N. Biomaterials based strategies for skeletal muscle tissue engineering: existing technologies and future trends. Biomaterials **53,** 502, 2015.
27. Liu, J., Saul, D., Boker, K.O., Ernst, J., Lehman, W., and Schilling, A.F. Current methods for skeletal muscle tissue repair and regeneration. Biomed Res Int **2018,** 1984879, 2018.
28. Passipieri, J.A., and Christ, G.J. The potential of combination therapeutics for more complete repair of volumetric muscle loss injuries: the role of exogenous growth factors and/or progenitor cells in implantable skeletal muscle tissue engineering technologies. Cells Tissues Organs **202,** 202, 2016.
29. Badylak, S.F., Dziki, J.L., Sicari, B.M., Ambrosio, F., and Boninger, M.L. Mechanisms by which acellular biologic scaffolds promote functional skeletal muscle restoration. Biomaterials **103,** 128, 2016.
30. Pantelic, M.N., and Larkin, L.M. Stem cells for skeletal muscle tissue engineering. Tissue Eng Part B Rev **24,** 373, 2018.
31. Corona, B.T., Machingal, M.A., Criswell, T., *et al.* Further development of a tissue engineered muscle repair construct in vitro for enhanced functional recovery following implantation in vivo in a murine model of volumetric muscle loss injury. Tissue Eng Part A **18,** 1213, 2012.
32. Corona, B.T., Ward, C.L., Baker, H.B., Walters, T.J., and Christ, G.J. Implantation of in vitro tissue engineered muscle repair constructs and bladder acellular matrices partially restore in vivo skeletal muscle function in a rat model of volumetric muscle loss injury. Tissue Eng Part A **20,** 705, 2014.
33. Machingal, M.A., Corona, B.T., Walters, T.J., *et al.* A tissue-engineered muscle repair construct for functional restoration of an irrecoverable muscle injury in a murine model. Tissue Eng Part A **17,** 2291, 2011.
34. Passipieri, J.A., Hu, X., Mintz, E., *et al.* In silico and in vivo studies detect functional repair mechanisms in a volumetric muscle loss injury. Tissue Eng Part A **25,** 1272, 2019.
35. Passipieri, J.A., Baker, H.B., Siriwardane, M., *et al.* Keratin hydrogel enhances in vivo skeletal muscle function in a rat model of volumetric muscle loss. Tissue Eng Part A **23,** 556, 2017.
36. Mintz, E.L., Passipieri, J.A., Lovell, D.Y., and Christ, G.J. Applications of in vivo functional testing of the rat tibialis anterior for evaluating tissue engineered skeletal muscle repair. J Vis Exp [Epub ahead of print]; DOI: 10.3791/54487, 2016.
37. Deveci, D., and Egginton, S. Differing mechanisms of cold-induced changes in capillary supply in m. tibialis anterior of rats and hamsters. J Exp Biol **205,** 829, 2002.
38. Corona, B.T., Wu, X., Ward, C.L., McDaniel, J.S., Rathbone, C.R., and Walters, T.J. The promotion of a functional fibrosis in skeletal muscle with volumetric muscle loss injury following the transplantation of muscle-ECM. Biomaterials **34,** 3324, 2013.
39. Deveci, D., Marshall, J.M., and Egginton, S. Chronic hypoxia induces prolonged angiogenesis in skeletal muscles of rat. Exp Physiol **87,** 287, 2002.
40. Armstrong, R.B., and Phelps, R.O. Muscle fiber type composition of the rat hindlimb. Am J Anat **171,** 259, 1984.
41. Kang, S.B., Olson, J.L., Atala, A., and Yoo, J.J. Functional recovery of completely denervated muscle: implications for innervation of tissue-engineered muscle. Tissue Eng Part A **18,** 1912, 2012.
42. Mann, C.J., Perdiguero, E., Kharraz, Y., *et al.* Aberrant repair and fibrosis development in skeletal muscle. Skelet Muscle **1,** 21, 2011.
43. Brown, B.N., Valentin, J.E., Stewart-Akers, A.M., McCabe, G.P., and Badylak, S.F. Macrophage phenotype and remodeling outcomes in response to biologic scaffolds with and without a cellular component. Biomaterials **30,** 1482, 2009.
44. Baker, H.B., Passipieri, J.A., Siriwardane, M., *et al.* Cell and growth factor-loaded keratin hydrogels for treatment of volumetric muscle loss in a mouse model. Tissue Eng Part A **23,** 572, 2017.
45. Ward, C.L., Ji, L., and Corona, B.T. An autologous muscle tissue expansion approach for the treatment of volumetric muscle loss. Biores Open Access **4,** 198, 2015.
46. Grasman, J.M., Do, D.M., Page, R.L., and Pins, G.D. Rapid release of growth factors regenerates force output in volumetric muscle loss injuries. Biomaterials **72,** 49, 2015.
47. McClure, M.J., Cohen, D.J., Ramey, A.N., *et al.* Decellularized muscle supports new muscle fibers and improves function following volumetric injury. Tissue Eng Part A **24,** 1228, 2018.
48. Westman, A.M., Dyer, S.E., Remer, J.D., Hu, X., Christ, G.J., and Blemker, S.S. A coupled framework of in situ and in silico analysis reveals the role of lateral force transmission in force production in volumetric muscle loss injuries. J Biomech **85,** 118, 2019.
49. Gordon, T., and de Zepetnek, J.E.T. Motor unit and muscle fiber type grouping after peripheral nerve injury in the rat. Exp Neurol **285,** 24, 2016.
50. Deveci, D., Marshall, J.M., and Egginton, S. Relationship between capillary angiogenesis, fiber type, and fiber size in chronic systemic hypoxia. Am J Physiol Heart Circ Physiol **281,** H241, 2001.
51. Anderson, S.E., Han, W.M., Srinivasa, V., *et al.* Determination of a critical size threshold for volumetric muscle loss in the mouse quadriceps. Tissue Eng Part C Methods **25,** 59, 2019.
52. Arnold, L., Henry, A., Poron, F., *et al.* Inflammatory monocytes recruited after skeletal muscle injury switch into antiinflammatory macrophages to support myogenesis. J Exp Med **204,** 1057, 2007.
53. Huleihel, L., Dziki, J.L., Bartolacci, J.G., *et al.* Macrophage phenotype in response to ECM bioscaffolds. Semin Immunol **29,** 2, 2017.
54. Brown, B.N., Sicari, B.M., and Badylak, S.F. Rethinking regenerative medicine: a macrophage-centered approach. Front Immunol **5,** 510, 2014.

55. Brown, B.N., Londono, R., Tottey, S., *et al.* Macrophage phenotype as a predictor of constructive remodeling following the implantation of biologically derived surgical mesh materials. Acta Biomater **8,** 978, 2012.
56. Valentin, J.E., Stewart-Akers, A.M., Gilbert, T.W., and Badylak, S.F. Macrophage participation in the degradation and remodeling of extracellular matrix scaffolds. Tissue Eng Part A **15,** 1687, 2009.
57. Meng, F.W., Slivka, P.F., Dearth, C.L., and Badylak, S.F. Solubilized extracellular matrix from brain and urinary bladder elicits distinct functional and phenotypic responses in macrophages. Biomaterials **46,** 131, 2015.
58. Honda, H., Kimura, H., and Rostami, A. Demonstration and phenotypic characterization of resident macrophages in rat skeletal muscle. Immunology **70,** 272, 1990.
59. Tidball, J.G. Regulation of muscle growth and regeneration by the immune system. Nat Rev Immunol **17,** 165, 2017.

Address correspondence to:
George J. Christ, PhD
Department of Biomedical Engineering
University of Virginia
MR5, 415 Lane Road, Room 1133
Charlottesville, VA 22908-0904

E-mail: gjc8w@virginia.edu

Received: May 7, 2019
Accepted: August 13, 2019
Online Publication Date: January 23, 2020